Effect of Under-Cured HTPB in APCP has on Burn Behavior

Justin Sadler[1]

Florida Institute of Technology, Melbourne, Florida 32901, United States

Hydroxyl-terminated polybutadiene (HTPB) is widely used as a binder in ammonium perchlorate composite propellants (APCP) due to its favorable mechanical properties and processability. Propellants made with HTPB cure through a chemical reaction with a curative such as methylene diphenyl diisocyanate (MDI). HTPB's hydroxyl (-OH) group bonds with MDI's isocyanate (-NCO) groups to form a urethane linkage, creating a crosslinked rubber network. MDI provides strong mechanical and adhesive properties relative to other curatives, however, cure quality in HTPB-MDI systems is highly dependent on adequate mixing and is sensitive to moisture contamination. If not adequately addressed, these limitations can result in under-cured propellant exhibiting burn behavior different from that of fully cured material. This work investigates the effects that under-cured propellant has on the burn behavior resulting from poor mixing of the curative into the binder.

I.Nomenclature

A_t = throat area
A_{port} = port area
a = burn rate coefficient
f = generic functions
G = mass flux
g_c = dimensional conversion constant
$\dot{m}$ = mass flow rate
$\dot{m}_d$ = mass discharge rate
$\dot{m}_g$ = mass generated rate
n = pressure exponent
P_c = chamber pressure
$\dot{r}$ = linear burn rate
S = burning surface area
ρ_b = propellant density

[1] Undergraduate Student, Department of Aerospace, Physics, and Space Sciences, and AIAA Student Member (1740364)

II.Introduction

Ammonium perchlorate composite propellant (APCP) is a heterogeneous energetic material consisting of solid ammonium perchlorate oxidizer particles dispersed within a crosslinked polymeric binder. Achieving uniform dispersion of constituents and proper incorporation of the curing agent is imperative to obtaining consistent mechanical properties and predictable combustion behavior. During manufacturing, liquid constituents are typically mixed first, followed by incremental addition of solid oxidizer particles, often starting with larger particles to promote efficient packing. This process produces a highly viscous composite requiring significant shear for adequate homogenization. The final stage of processing involves incorporating a curing agent, which initiates crosslink formation and ultimately defines the material's mechanical properties. Once introduced, the mixture possesses a finite pot life, limiting the available time for casting.

During fabrication, a processing deviation occurred, resulting in incomplete dispersion of the curing agent, leading to regions of reduced crosslink density and non-uniform cure throughout the batch. This condition provided an opportunity to investigate the influence of incomplete curing on combustion characteristics.

This study examines how incomplete cure in APCP influences burn rate behavior and compares the measured performance to predictions for a fully cured propellant.

A. APCP Composition and Binder Chemistry

Ammonium perchlorate composite propellants (APCP) are among the most widely used solid rocket propellants. APCP is a heterogeneous particulate composite material consisting of discrete oxidizer and metal fuel particles embedded within a continuous polymeric binder matrix, typically hydroxyl-terminated polybutadiene (HTPB). Aluminum powder is commonly incorporated to increase flame temperature and overall energetic performance. Additional constituents may include processing aids to improve manufacturability, curatives to promote polymer network formation, and crosslinking aids to modify mechanical properties and network structure.

HTPB serves both as a fuel and as the structural binder that holds the particulate constituents together. The polymer backbone contains varying cis, trans, and vinyl configurations, which influence mechanical behavior and cure characteristics. HTPB chains terminate with hydroxyl (-OH) functional groups that react with isocyanate (-NCO) groups in a curative, most commonly methylene diphenyl diisocyanate (MDI). This reaction forms urethane linkages, creating a three-dimensional crosslinked polymer network.[1]

The extent of this reaction establishes the crosslink density, which governs the mechanical strength, stiffness, and thermal response of the binder system. In the present formulation, a multifunctional crosslinking aid, castor oil, was incorporated to increase network connectivity and enhance mechanical properties. These systems rely on near-complete hydroxyl-isocyanate reactions to achieve the intended crosslink density.

The mechanical properties of the binder strongly influence combustion behavior. Crosslink density affects particle retention, surface regression stability, and resistance to erosive forces during burning. Variations in cure extent or network uniformity may alter surface roughness evolution and burning rate characteristics, potentially impacting chamber pressure response.

B. APCP Combustion Process

Combustion of APCP is commonly described using a five-step model consisting of coupled condensed-phase and gas-phase processes. The first step involves endothermic decomposition within the condensed phase, where ammonium perchlorate (AP) undergoes thermal dissociation, and the HTPB binder begins pyrolysis. The second step consists of further exothermic AP decomposition reactions near the propellant surface. Above the surface, the third step is characterized by an exothermic premixed reaction of AP decomposition products, often referred to as the AP monopropellant flame. The fourth step corresponds to the primary diffusion flame, where oxidizer-rich gases from AP decomposition react with fuel-rich species originating from binder pyrolysis. The fifth and final step is a secondary diffusion or cleanup flame region, where remaining intermediate species are completely oxidized.[2]

Other formulation constituents, including processing aids and crosslinking agents, decompose and combust within these combustion zones. Aluminum introduces an additional heterogeneous metal combustion process that occurs primarily within and above the primary and secondary diffusion flame regions. Aluminum particles melt, ignite, and burn in the gas phase, contributing significant energy release and increasing overall flame temperature.

C. Burn Rate Modeling

The heat feedback from these gas-phase flame zones to the condensed phase governs the steady-state regression rate of the propellant surface. The burning rate, defined as the linear regression speed of the propellant surface, is commonly described by Saint Robert's Law:

$$\dot{r} = a * P_c^n \tag{1}$$

Where $\dot{r}$ is the linear burn rate, a is the burn rate coefficient, P_c is chamber pressure, and n is the pressure exponent. The pressure exponent governs the sensitivity of the regression rate to changes in chamber pressure and plays a critical role in determining motor stability.[3]

D. Erosive Burning Effects

The burn rate of a solid propellant may be augmented by a phenomenon known as erosive burning. Erosive burning refers to an increase in regression rate caused by high-velocity combustion gases flowing parallel to the propellant surface. This effect is typically localized within port passages and regions of elevated mass flux, such as near the nozzle entrance or in narrow grain geometries. Under severe conditions, erosive burning can significantly alter motor performance and may contribute to chamber over-pressurization.

To account for this behavior, the classical pressure-dependent burn rate relation may be modified to include a mass flux term:

$$\dot{r} = a * P_c^n + f(G) \tag{2}$$

Where G represents the local mass flux. This additional term accounts for enhanced convective heat transfer resulting from increased axial gas velocity. Higher gas velocities reduce the thickness of the thermal boundary layer at the propellant surface, increasing surface heat flux. This elevated heat feedback accelerates condensed-phase decomposition, producing a local regression rate greater than that predicted by pressure dependence alone. The magnitude of erosive burning is strongly dependent on mass flux, grain geometry, and surface characteristics, all of which may be influenced by binder mechanical properties and cure state.

$$G = \frac{\dot{m}}{A_{port}} \tag{3}$$

Mass flux is represented by the mass flow rate $\dot{m}$ per area of the port, A_t. The onset of erosive burning due to mass flux is typically defined as greater than 1, but it is pressure dependent, with higher pressure being less affected by erosive burning.[4]

E. Internal Ballistics and Pressure Prediction

Chamber pressure in a solid rocket motor may be estimated using mass conservation, where the rate of gas generation at the burning surface is equal to the mass flow rate discharged through the nozzle. The mass generation rate is given by:

$$\dot{m}_g = \dot{r} * S * \rho_b \tag{4}$$

where ρ_b is the propellant density, $\dot{r}$ is the linear burn rate, and S is the burning surface area. For choked nozzle flow, the mass discharge rate is expressed as:

$$\dot{m}_d = P_c * A_t * g_c / C^* \quad (5)$$

where P_c is chamber pressure, A_t is throat area, g_c is the dimensional conversion constant required for consistency in English engineering units, and C^* is the characteristic velocity.

Equating mass generation and discharge and substituting the pressure-dependent burn rate relations, chamber pressure can be written as:

$$P_c = [a * S * \rho_b * C^* / A_t * g_c]^{1/(1-n)} \quad (6)$$

This relation illustrates that chamber pressure is strongly dependent on burning surface area, throat area, and the pressure exponent n.[5]

For a BATES grain configuration, grain geometry evolution may be estimated using the linear burn rate. The radial regression rate of the internal port equals $\dot{r}$, and axial regression occurs at a rate of $2\dot{r}$ due to burning from both exposed end faces.

F. Literature Context and Research Gap

While internal ballistics models can accurately predict chamber pressure under ideal steady-state conditions, deviations may arise from unmodeled erosive effects, assumptions regarding uniform geometry evolution, or variations in material properties. Although erosive burning and pressure-coupled regression behavior are well documented in literature, comparatively fewer studies have directly examined the influence of binder cure state and crosslink density variations on measurable chamber pressure deviations in small-scale solid rocket motors. These considerations motivate experimental evaluation of material-dependent deviations from classical internal ballistics predictions.

Consequently, the present study investigates chamber pressure behavior in a small-scale APCP motor to evaluate potential contributions from erosive burning and cure-state-dependent material effects.

III.Methodology

A. Propellant formulation and processing

The propellant formulation used in this work consisted of ammonium perchlorate (AP) oxidizer, aluminum fuel, and a hydroxyl-terminated polybutadiene (HTPB) binder cured with methylene diphenyl diisocyanate (MDI), along with minor additives to aid processing and mechanical performance.

The oxidizer content was 75% by mass and comprised a bimodal particle size distribution of 200 μm and 90 μm AP to enhance packing efficiency and solids loading. Aluminum powder with an average particle size of 20 μm constituted 7.5% by mass. The binder system included 10.88% HTPB and 1.94% MDI curative. The remaining 4.68% consisted of isodecyl pelargonate (IDP) plasticizer, castor oil as a multifunctional crosslinking aid, and additional processing additives to improve mix homogeneity and castability.

All propellant used in this study was produced in a single batch of approximately 10 lb. Initial mixing of the binder and metallic fuel proceeded without complication. However, incorporation of the AP oxidizer presented processing challenges due to increased viscosity and mixer capacity limitations relative to batch size. The oxidizer was introduced incrementally over an extended mixing period to promote uniform particle dispersion. Intermittent pauses in mixing were required to prevent overheating of the mixing equipment.

Upon addition of the MDI curative, the viscosity of the mixture was at its highest at this stage, limiting the mixability of the mixture. Unlike earlier mixing stages, extended incremental mixing was not feasible during the cure initiation phase. As a result, complete homogenization of the curative distribution may not have been achieved. This processing limitation likely resulted in spatial variations in cure extent and local crosslink density throughout the batch.

The propellant slurry was manually packed into cylindrical plastic molds lined with polytetrafluoroethylene (PTFE) film to facilitate demolding. Grains were cured at ambient laboratory conditions for five days prior to removal from the molds.

Following demolding, qualitative assessment of the cured grains indicated incomplete cure development. The propellant surface exhibited a persistent tacky texture, and the material demonstrated reduced stiffness relative to nominal fully cured APCP formulations. Surface indentations and handling marks were easily introduced under light manual pressure, indicating reduced elastic modulus and insufficient network formation.

These observations are consistent with incomplete reaction between hydroxyl functional groups in the HTPB binder and isocyanate groups in the MDI curative. Given the mixing constraints described previously, incomplete homogenization of the curative likely resulted in spatially varying crosslink density throughout the propellant grains. The resulting under-cured material condition is expected to influence mechanical integrity, surface regression behavior, and resistance to erosive flow during combustion.

B. Motor Configuration

The experimental motor utilized a reusable carbon fiber composite case with an internal diameter of 2.0 in and an overall length of 14.5 in. The forward closure was retained by an integral bonded retaining lip, while the nozzle was secured using an internal snap-ring. The case was designed for repeated use with minor cleaning between firings.

The motor was loaded with three Bates grains. Each grain has an outer diameter of 1.775 in, an initial internal port diameter of 0.75 in, and a length of 3.0 in. Grains were cast in 3D-printed cylindrical molds and subsequently bonded into a linen phenolic liner using an epoxy adhesive.

The nozzle was fabricated from graphite and incorporated a conical converging-diverging geometry. The throat diameter was 0.40 in, and the exit diameter was 1.25 in. The converging section had a half-angle of 75 °, and the diverging section had a half-angle of 15 °.

C. Static Fire Testing Procedure

The motor was ignited using an electric match (e-match) augmented with a small quantity of loose propellant affixed to the igniter tip. This promoted rapid ignition and flame spread across the exposed grain surfaces.

All tests were conducted in a vertical orientation, with the motor nozzle directed upward and the motor restrained against the ground to prevent movement during operation. This configuration minimized structural loading of the case and ensured consistent axial alignment during firing.

Ambient temperature varied slightly between test events but remained within the 80°F range for all firings. No active environmental control was implemented, as tests were performed outside.

A total of four static fire tests were conducted using propellant grains from the same batch. Visual post-fire inspection of the motor hardware and recovered components revealed no apparent structural anomalies or catastrophic material failures. Combustion appeared nominal in all tests based on external observation.

Chamber pressure data were recorded using an Altus Metrum EasyMotor data acquisition system at a sampling interval of 0.01 s (100 Hz). Raw pressure traces were exported for post-processing and analysis.

Burn duration was defined using a pressure threshold method. Specifically, burn start and end times were determined as the points at which chamber pressure exceeded and subsequently fell below 10% of the recorded peak pressure for each test. Data outside this threshold were excluded from burn time and performance metric calculations.

Average chamber pressure was computed over the defined burn duration. Peak pressure was identified as the maximum recorded pressure value within the burn window. Total impulse was calculated via numerical integration of the calculated thrust from the chamber pressure over the burn duration, assuming quasi-steady nozzle flow conditions.

D. Internal Ballistics Simulation Model

A quasi-steady internal ballistics model was developed in MATLAB to predict chamber pressure as a function of time. The governing relations were based on mass conservation, equating the propellant mass generation rate to the choked nozzle mass discharge rate. The burn rate was modeled using the classical Saint Robert's law. Burn rate parameters were selected based on representative values for the APCP formulation with identical composition.

Table 1. Internal Ballistics Model Parameters

Parameter	Symbol	Value	Units
Burn rate coefficient	a	0.024986	$in/(s \cdot psi^n)$
Pressure exponent	n	0.327300	—
Characteristic velocity	C*	5000	ft/s
Propellant density	ρ	0.060333	lb/in^3

The model assumed quasi-steady, spatially uniform regression and did not include erosive burning augmentation or transient ignition effects. The calculated mass flux of the motor simulated was 0.76 lb/in^2, which is under the known onset of erosive burning. Characteristic velocity C* was assumed to be constant throughout the burn.

Grain geometry evolution was computed dynamically at each integration step. For the BATES configuration, radial regression of the internal port regressed at a rate $\dot{r}$, while axial regression from both exposed end faces was applied at $2\dot{r}$. The instantaneous burning surface area was recalculated at each time step.

The governing differential equation for chamber pressure was integrated numerically using MATLAB's ODE45 solver. Simulation results were cross-validated against publicly available internal ballistics software and demonstrated agreement under identical geometric and material assumptions.

IV.Results

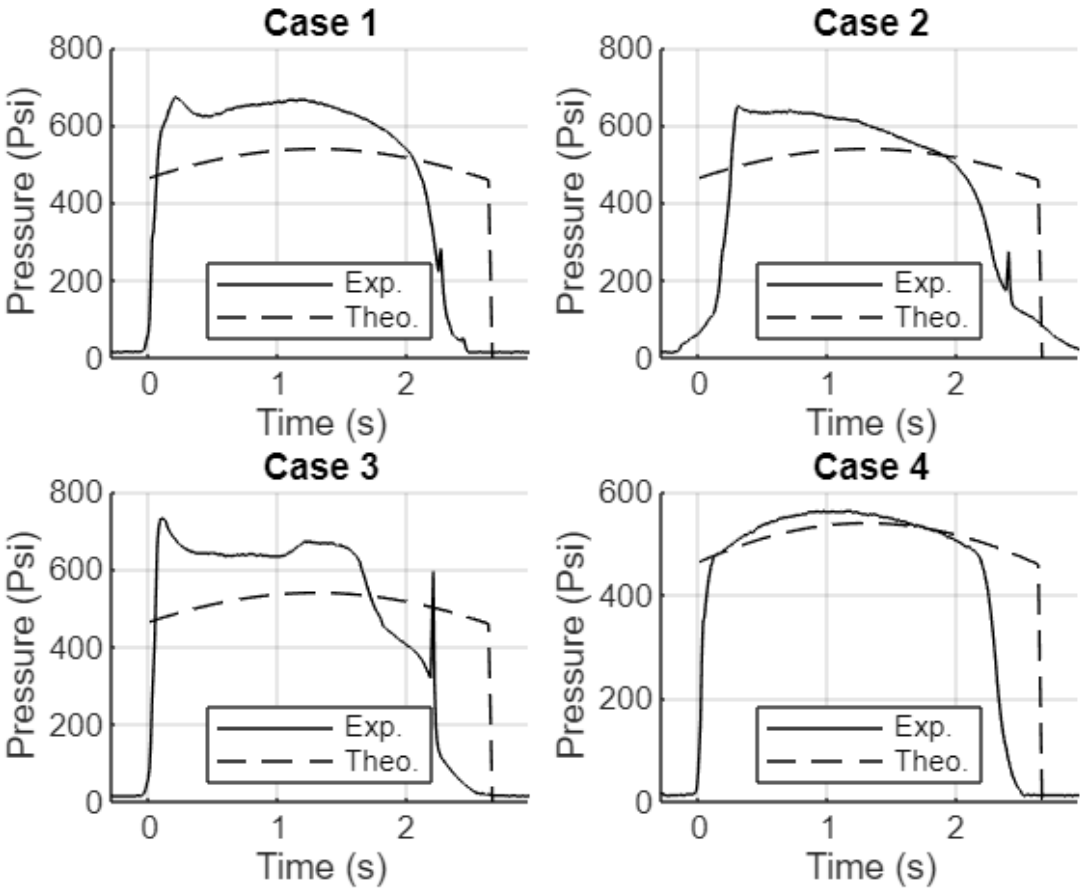

Figure 1. Chamber pressure versus time for four static fire tests compared with simulation. Static fires were collected as experimental (exp.) data, and the simulations were used as theoretical (theo.) data.

Table 2. Summary of results from static fires.

	Burn Time (s)	Average Pressure (psi)	Peak Pressure (psi)	Total Impulse (lbf-s)
Case 1	2.36	521.23	672.30	195.80
Case 2	2.74	421.38	648.16	181.86
Case 3	2.37	500.71	730.62	189.18
Case 4	2.44	449.50	561.69	173.32
Simulation	2.67	505.63	538.28	194.12

Table 3. Deviation of experiments from simulation.

	Exp. Average	Standard Deviation	% uncertainty	Simulation	Percent Error
Burn Time (s)	2.48	0.18	7.25	2.67	7.66
Average Pressure (psi)	473.21	45.86	9.69	505.63	6.85
Peak Pressure (psi)	653.19	70.13	10.74	538.28	17.59
Total Impulse (lbf-s)	185.04	9.67	5.23	194.12	4.91

The simulation predictions were compared to the average values obtained from four static fire tests. Burn time was predicted within 7.66% of the experimental mean, which is comparable to the measured experimental variability of 7.25%, indicating close agreement between modeled and observed regression duration.

Average chamber pressure was predicted within 6.85% of the experimental mean and falls within the measured experimental variability of 9.69%, demonstrating strong agreement in mean chamber pressure prediction.

Peak chamber pressure was underpredicted by 17.59%, which exceeds the experimental variability of 10.74%. This indicates reduced predictive accuracy of the model with respect to maximum chamber pressure compared to integrated performance metrics.

Total impulse was predicted within 4.9% of the experimental mean and falls within the measured experimental variability of 5.1%, demonstrating strong agreement in overall integrated motor performance.

Overall, the simulation demonstrated good agreement for burn duration, average chamber pressure, and total impulse, while exhibiting larger deviation in peak chamber pressure prediction.

V.Discussion

The following discussion evaluates potential mechanisms responsible for the observed peak pressure deviation. The 17.6% underprediction in peak chamber pressure indicates that the experimental motor produced higher instantaneous mass generation rates than predicted by the nominal internal ballistics model. Because burn duration, average pressure, and total impulse were predicted within experimental variability, the discrepancy appears primarily associated with transient peak pressure development rather than global energetic output.

One plausible contributor is the under-cured condition of the propellant. Qualitative observations indicated reduced stiffness and incomplete network formulation, suggesting lower crosslink density relative to a fully cured formulation. Reduced mechanical strength can increase susceptibility to microcracking under pressurization and thermal loading. The formation of cracks or surface fissures would locally increase burning surface area, resulting in elevated instantaneous mass generation and higher peak chamber pressure.

Additionally, the cure state may influence regression behavior through changes in mechanical response at the burning surface. A softer binder matrix may deform or erode more readily under internal flow, potentially amplifying localized regression rates. Although the chemical decomposition of HTPB requires bond scission of the hydroxyl-isocyanate

crosslinks, this process is not expected to be rate-limiting compared to mechanical and thermal processes governing surface regression. Therefore, mechanical effects associated with incomplete cure are considered a more likely contributor to the observed peak pressure deviation.

Alternative explanations should also be considered. Variations in cure state may alter intrinsic burn rate parameters, including burn rate coefficient a and the pressure exponent n. Localized differences in crosslink density could therefore increase the effective pressure sensitivity of the propellant, resulting in elevated peak pressure without significantly altering performance metrics.

It should be noted that erosive burning was not included in the simulation model. Increased port flow velocity in combination with reduced material stiffness could further enhance surface regression near peak pressure conditions, contributing to the observed discrepancy. As seen in Figure 1, cases 1 and 3 had an initial pressure spike that mimics how erosive burning would look, suggesting the possibility that under-cured propellant is more susceptible to erosive burning, and the onset occurs at a lower mass flux.

Variations in the pressure curves from case to case suggest that each grain had varying crosslink density, giving different burn properties. Case 4 was the closest to the sims, matching very closely, while the other three cases had obvious deviations. No direct mechanical characterization was performed on the propellant, so conclusions on crosslink density remain qualitative.

VI.Conclusion

The study evaluated the combustion behavior of an under-cured ammonium perchlorate composite propellant through static fire testing and comparison with a quasi-steady internal ballistics simulation. The propellant batch exhibited qualitative indicators of incomplete cure, including persistent surface tackiness and reduced mechanical stiffness.

Simulation predictions showed strong agreement with experimental burn duration (7.67% deviation), average pressure (6.85% deviation), and total impulse (4.9% deviation), all three within measured experimental variability. These results indicate that the global energetic output of the propellant was adequately captured by a classical internal ballistics model using nominal burn rate parameters and constant characteristic velocity assumptions.

However, peak chamber pressure was underpredicted by 17.6%, exceeding experimental variability. This discrepancy suggests that while integrated performance metrics were well represented, transient pressure development was not fully captured by the model. The results are consistent with the hypothesis that reduced mechanical integrity associated with incomplete cure may enhance localized burning surface area through cracking or deformation, leading to elevated instantaneous mass generation rates. The results also suggested that under-cured propellant is more susceptible to erosive burning, and the onset occurs at a lower mass flux than that of fully cured propellant.

Overall, the findings demonstrate that under-cured APCP propellant may exhibit combustion behavior that deviates from classical quasi-steady prediction primarily in peak pressure characteristics rather than total impulse. These results highlight the importance of the cure state in influencing transient internal ballistics behavior and underscore the need to consider mechanical property effects when modeling propellant regression under pressurized conditions.

VII.References

[1] H. Arisawa, and T.B. Brill. “Flash pyrolysis of hydroxyl-terminated polybutadiene (HTPB) I: Analysis and implications of the gaseous products.” *Combustion and Flame*, vol. 106, no. 1–2, July 1996, pp. 131–143, https://doi.org/10.1016/0010-2180(96)00253-2.

[2] Dennis, Claresta, and Brian Bojko. “On the combustion of heterogeneous AP/HTPB composite propellants: A Review.” *Fuel*, vol. 254, Oct. 2019, p. 115646, https://doi.org/10.1016/j.fuel.2019.115646.

[3] *Richard Nakka’s Experimental Rocketry Site*, www.nakka-rocketry.net/burnrate.html. Accessed 25 Feb. 2026.

[4] “Welcome to Rasaero.Com.” *Welcome to RASAero.Com*, rasaero.com/. Accessed 25 Feb. 2026.

[5] Shekhar, Himanshu. “Estimation of pressure index and temperature sensitivity coefficient of solid rocket propellants by Static Evaluation.” *Defence Science Journal*, vol. 59, no. 6, 24 Nov. 2009, pp. 666–669, https://doi.org/10.14429/dsj.59.1573.